ESTIMATION OF RAINDROP SIZE DISTRIBUTION FROM POLARIMETRIC RADAR MEASUREMENTS AT ATTENUATIONG FREQUENCY BASED ON THE SELF-CONSISTENCY PRINCITPE

4B.4

Ahoro Adachi[1)]*, Takahisa Kobayashi[2),1)] and Hiroshi Yamauchi[1)]
[1)]MRI, Tsukuba, Japan, [2)]CRIEPI, Abiko, Japan

1. INTRODUCTION

Accurate characterization of raindrop size distribution (DSD) and the estimation of DSD parameters over large spatial and temporal scales is a long-standing goal for the studies based on polarimetric radar measurements (e.g., Gorgucci et al. 2008). Indeed, many studies have proposed methods to estimate DSD parameters as a part of rainfall rate estimation algorithms. However, most of those methods require external reference data such as 2DVD measurements to derive relations that are essential for the DSD parameter retrieval algorithms (e.g., Gorgucci et al. 2002; Brandes et al. 2003; Kalogiros et al. 2013). Making use of the physical-based ad hoc or empirical relations derived from the reference data may cause error because of the raindrop temperature, shape, and size distribution dependency when used in different conditions, including seasons, locations, and precipitation types. Moreover, the fact that the sampling volume of the reference data is quite different from that of radar makes it difficult to obtain reliable reference data. Therefore, a DSD retrieval algorithm that does not require external reference DSD data is needed to estimate DSD parameters and rainfall rate from polarimetric measurements with high reliability.

In the present study, we propose a new algorithm to estimate the three DSD parameters and rainfall rate for polarimetric radar at the attenuation frequency using consistency among the polarimetric measurements. The proposed algorithm requires no external reference data such as 2DVD measurements for attenuation corrections because it retrieves co-polar and differential specific attenuation from the interrelation among the polarimetric measurements.

2. METHODOLOGY

The attenuation correction algorithm used in the present study assumes that the raindrop temperature and operating frequency are given and that all polarimetric variables including attenuation are determined by the DSD, which is represented by the modified gamma distribution. Also, no ice hydrometeors (such as hail and/or graupel) are assumed to be included in the range profile. The attenuation-corrected Z_H and Z_{DR} obtained with the proposed method are used to derive the three DSD parameters, i.e., the shape parameter μ, the median volume diameter D_0, and the raindrop concentration N_0 as shown below.

2.1 *Attenuation Correction*

Horizontal reflectivity Z_H and vertical reflectivity Z_V can be expressed in terms of the raindrop concentration N_0 as

$$Z_{H,V} = N_0 \times F_{H,V}(\mu, D_0), \quad (1)$$

where

$$F_{H,V}(\mu, D_0) = 10^{18} \times \frac{\lambda^4}{\pi^5 |K|^2} \int_{D_{min}}^{D_{max}} 4\pi \left|S_{hh,vv}(D)\right|^2 D^\mu \exp\left(-\frac{3.67+\mu}{D_0} D\right) dD. \quad (2)$$

Note in the derivation of Eq. (1), N_0 was moved from the inside of integral in Eq. (2) to the first term of Eq. (1) because N_0 is a constant and is independent of D.

The differential reflectivity, Z_{DR} is given from Eq. (1) by

$$Z_{DR} = 10 \log_{10}\left(\frac{N_0 \times F_H(\mu, D_0)}{N_0 \times F_V(\mu, D_0)}\right) \equiv G_{DR}(\mu, D_0). \quad (3)$$

Equation (3) clearly shows that Z_{DR} is independent of N_0. Similarly, the specific attenuation of horizontal polarization A_H can be expressed in terms of N_0 as

$$A_H = N_0 \times B_H(\mu, D_0), \quad (4)$$

where

$$B_H(\mu, D_0) = 8.686 \times 10^3 \lambda \times \operatorname{Im} \int_{D_{min}}^{D_{max}} f_{hh}(D) D^\mu \exp\left(-\frac{3.67+\mu}{D_0} D\right) dD. \quad (5)$$

Additionally, the differential specific attenuation A_{DP} can also be expressed in terms of N_0 as

$$A_{DP} = N_0 \times B_{DP}(\mu, D_0), \quad (6)$$

where

$$B_{DP}(\mu, D_0) = 8.686 \times 10^3 \lambda \times \operatorname{Im} \int_{D_{min}}^{D_{max}} \left\{f_{hh}(D) - f_{vv}(D)\right\} D^\mu \exp\left(-\frac{3.67+\mu}{D_0} D\right) dD. \quad (7)$$

* *Corresponding author address:* Ahoro Adachi, Meteorological Research Institute, Meteorological Satellite and Observation System Research Dept., Tsukuba, 305-0052 Japan; e-mail: aadachi(at)mri-jma.go.jp

The terms of A_H/Z_H and A_{DP}/Z_H are given from Eqs. (1), (4), and (6) by

$$\frac{A_H}{Z_H} = \frac{N_0 \times B_H(\mu, D_0)}{N_0 \times F_H(\mu, D_0)} \equiv L_H(\mu, D_0), \tag{8}$$

and

$$\frac{A_{DP}}{Z_H} = \frac{N_0 \times B_{DP}(\mu, D_0)}{N_0 \times F_H(\mu, D_0)} \equiv L_{DP}(\mu, D_0). \tag{9}$$

Eqs. (3), (8), and (9) show that both A_H/Z_H and A_{DP}/Z_H can be expressed as a function of Z_{DR} by use of D_0 as an intermediate variable for a given value of μ, as shown in Fig. 1.

Figure 1 indicates that the consistency curve of A_H/Z_H has low temperature and shape-parameter dependencies, especially for C-band. However, this figure also shows that the consistency curve of A_{DP}/Z_H has slightly larger dependencies not only on temperature but also on shape parameter, especially for X-band. These small dependencies on both temperature and shape parameter could make large differences in the retrieval of rainfall rate, particularly in heavy rainfall, because the attenuation effects are defined as path integrals of the co-polar and differential specific attenuation given by

$$Z_H^{obs}(r) = Z_H^{true}(r) - 2\int_{r_1}^{r} A_H(s)ds - C_H \tag{10}$$

and

$$Z_{DR}^{obs}(r) = Z_{DR}^{true}(r) - 2\int_{r_1}^{r} A_{DP}(s)ds - C_{DP}, \tag{11}$$

where $Z_H^{true}(r)$(dBZ) and $Z_{DR}^{true}(r)$(dB) represent true reflectivity and differential reflectivity after attenuation correction at a range of r, respectively, r_1 is the distance of the first range resolution volume, and C_H and C_{DP} are the correction terms for the reflectivity and differential reflectivity profiles, respectively.

We have opted for a simple gate-to-gate attenuation correction scheme based on (Aydin et al. 1989). The true reflectivity and differential reflectivity at range r_n can be obtained by recurrence formulas derived from Eqs. (10) and (11) as

$$Z_H^{true}(r_n) = Z_H^{obs}(r_n) + 2\sum_{k=1}^{n} A_H\left(Z_H^{true}(r_{k-1}), Z_{DR}^{true}(r_{k-1})\right)\delta s + C_H, \tag{12}$$

$$Z_{DR}^{true}(r_n) = Z_{DR}^{obs}(r_n) + 2\sum_{k=1}^{n} A_{DP}\left(Z_H^{true}(r_{k-1}), Z_{DR}^{true}(r_{k-1})\right)\delta s + C_{DP} \tag{13}$$

where r_n represents the distance of the nth range gate, δs (km) is the range resolution of the radar measurements and

$$A_H\left(Z_H^{true}(r_0), Z_{DR}^{true}(r_0)\right) = A_{DP}\left(Z_H^{true}(r_0), Z_{DR}^{true}(r_0)\right) = 0\ . \tag{14}$$

Note that the co-polar and differential specific attenuation are inferred from true Z_H and Z_{DR} with the consistency curves in Figs. 1a and 1b, respectively. The term C_{DP} is the sum of relative bias error in Z_{DR} and excess differential attenuation. In the method used here, it is also assumed that the systematic bias in Z_{DR} measurements is negligible (by calibrating with vertical measurements in rain) and that excess differential attenuation can be neglected assuming that both the H and V signal powers are affected almost equally by rain on the radome. Therefore, the value of C_{DP} is set to zero, as assumed in Bringi et al. (2006). Similarly, the bias (C_H) in the observed Z_H corrected with the proposed method is the sum of the radar constant calibration error and any excess attenuation from the radar to the first range resolution volume, including excess attenuation due to rain on the radome, as shown in Eqs. (12) and (14). Note that the value of C_H could vary with the beam direction and time because it contains excess attenuation due to the wet radome of the antenna. We estimated the value of C_H by use of the autocalibration of Z_H introduced by Goddard et al. (1994).

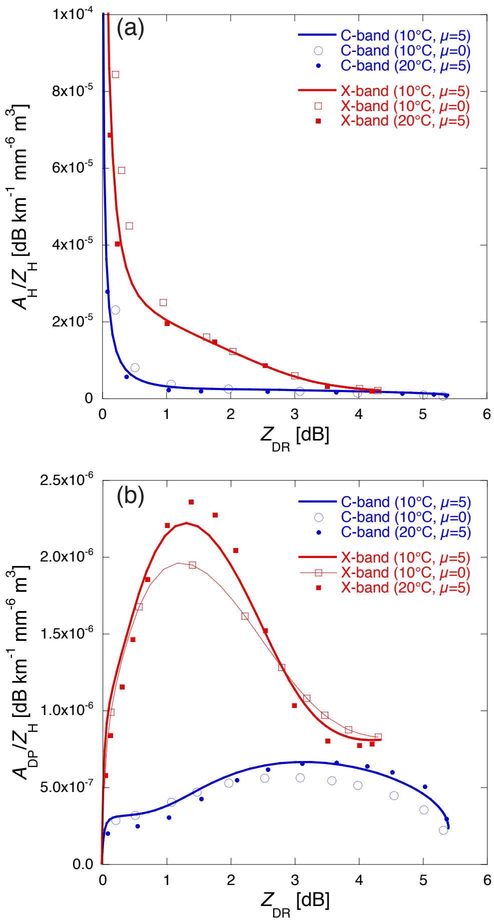

Fig. 1. (a) Relationships of horizontal specific attenuation per unit linear horizontal reflectivity and (b) specific differential attenuation per unit linear horizontal reflectivity as a function of differential reflectivity at raindrop temperatures of 10 °C and 20 °C at C-band (5.370 GHz) and X-band (9.375 GHz) with shape parameters of 0 and 5 for a modified gamma distribution with the axis ratio of Brandes et al. (2005).

2.2 *Retrieval of the DSD Parameters*

The DSD parameters are derived from the attenuation-corrected Z_H and Z_{DR} obtained with the proposed method. The shape parameter is estimated by comparing the theoretical Φ_{DP} with the smoothed-observed Ψ_{DP} through a rain path in the radial direction, as shown later in Section 3. Once the shape parameter is determined, the median volume diameter D_0 can be derived from the attenuation-corrected Z_{DR} at each range gate because Z_{DR} is independent of N_0 and is a function of D_0 and μ, as given by Eq. (3). Then, N_0 can be derived from the true Z_H with the retrieved D_0 and μ from Eq. (1). Other rain parameters including rainfall rate can be derived theoretically from the DSD parameters.

3. MRI C-BAND POLARIMETRIC RADAR AND RETRIEVAL OF DSD PARAMETERS

3.1. *MRI C-band Polarimetric Radar*

The Meteorological Research Institute (MRI) advanced C-band solid-state polarimetric radar (MACS-POL radar) is mounted on top of the MRI building in Tsukuba, Japan (Adachi et al. 2013). The radar routinely collects a full suite of dual-polarization measurements, including the reflectivity factor (Z_H), differential reflectivity (Z_{DR}), differential propagation phase (Ψ_{DP}), and correlation coefficient at zero lag ($\rho_{HV}(0)$). This system employs two solid-state amplifier units to transmit horizontally and vertically polarized waves. The radar is operating in the simultaneous transmission and reception (STAR) mode for polarized signals. Because the peak power of the amplifiers was slightly weak, observations were made with a long pulse to increase the mean power. A pulse compression technique with a linear FM chirp was used to increase range resolution. Because radar cannot observe in the vicinity of the antenna with long-pulse observations, this radar alternately transmitted short and long pulses to cover the blind region associated with the long-pulse observations. The operating frequencies deployed for the two pulses were separated to avoid mutual contamination. The configuration and operating parameters of the radar are summarized in Table 1.

Table 1. Operating characteristics of the MRI advanced C-band solid-state polarimetric radar.

Frequency	5370 MHz
Occupied band width	< 4.5 MHz
Peak power	3.5 kW (for each channel, simultaneous transmission)
Duty	20 % (Max)
Pulse length	1μs (range < 20 km) and 129 μs (≥ 20 km) for Elv. < 8° 1μs (range < 7.5 km) and 47 μs (≥ 7.5 km) for Elv. ≥ 8°
Pulse compression	Linear FM chirp for long-pulse observations
Antenna diameter	Parabolic dish, Φ = 4 m
Antenna speed	4 rpm for Elv. <8° and 6 rpm for Elv. ≥ 8°
Signal minimum	< –110 dBm
Antenna gain (H and V)	> 42 dBi
Max cross-polar isolation	< –40 dB
Beam width	1.01°
Azimuth spacing	0.7°
Transmitter	GaAs Power FET
Number of linear sampling	20
Range Gate Spacing	150 m
PRF	624/780 Hz (Elv. < 8°) and 936/1170 Hz (Elv. ≥ 8°)
Observation parameters	Z_H, Z_V, Z_{DR}, radial velocity, $\rho_{HV}(0)$ and Ψ_{DP}
Vendor	TOSHIBA

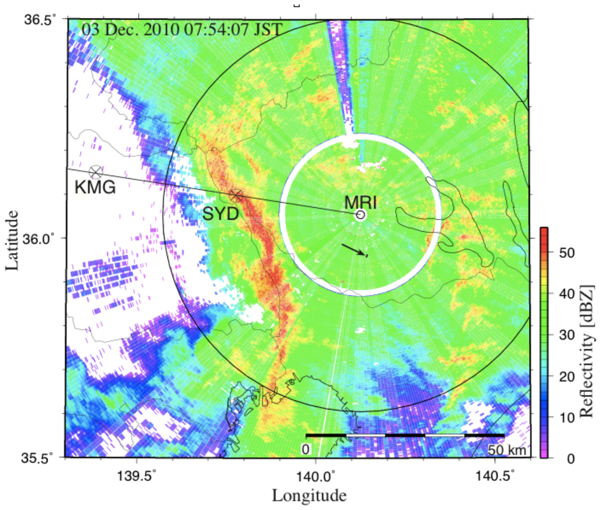

Fig. 2. Radar reflectivity field of the MRI C-band polarimetric radar at an elevation angle of 1.0° at 0754 JST on 3 December 2010. The color scale represents radar reflectivity in dBZ. The thick line in the figure depicts the direction of the radial profiles analyzed in Figs. 3 and 4, and the open circles with a cross on the line indicate the locations of the Sekiyado (SYD) and Kumagaya (KMG) surface observation stations. The arrow indicates the location of an F1 tornado formed at 0820 JST. The white circular band at 19–20.5 km from the radar is a deficit region resulting from the alternation of short- and long-pulse observations.

3.2. *Autocalibration and Retrievals of Rain Microphysical Parameters*

The radar reflectivity field observed by the MACS-POL radar at 0754 JST (Japan Standard Time: JST = UTC + 9 h) on 3 December 2010 indicates that a very heavy convective rain line was approaching the MRI site from the southwest with a speed of about 18 m s^{-1} (Fig. 2). This figure shows that the rain line passed at this time over Sekiyado (SYD), where a Parsivel optical disdrometer (Löffler-Mang and Joss 2000) was installed. Thus, we explore radial profiles of the radar data at an azimuth of 279° in the experiments so that the radial profile extends toward the Sekiyado site, as shown in the figure by the thick line.

Range profiles of observed Ψ_{DP}, running mean of observed Ψ_{DP}, and theoretical Φ_{DP} estimated from attenuation corrected Z and Z_{DR} with the proposed method are shown in Fig. 3. We applied a running mean to the observed Ψ_{DP} to mitigate the high frequency fluctuations including the backscatter differential phase δ and retain the mean trend for ease of viewing. Note that this running mean applied to the observed Ψ_{DP} does not have any influence on the theoretical estimations of Φ_{DP}. The values of measured Z were scaled so that the theoretical Φ_{DP} fits the smoothed-observed Ψ_{DP} with range using the autocalibration technique.

Figure 3 shows a good agreement with range between the smoothed-measured Ψ_{DP} and theoretical Φ_{DP} with attenuation correction procedures profiles.

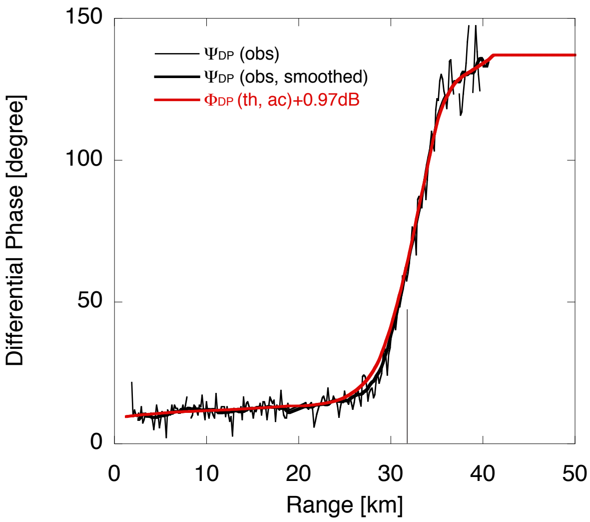

Fig. 3. Radial profiles of observed Ψ_{DP} (thin black line), observed Ψ_{DP} smoothed along 20 (=3 km) gates (thick black line), and theoretical Φ_{DP} (red) for the azimuth of 279° at 0754 JST on 3 December 2010. The theoretical Φ_{DP} profiles are obtained by assuming a raindrop temperature of 10 °C and a shape parameter of raindrops of 5. The light-blue vertical line indicates the location of a disdrometer at Sekiyado (31.8 km from the radar). The initial differential phase value of 9.5° is an arbitrary system offset.

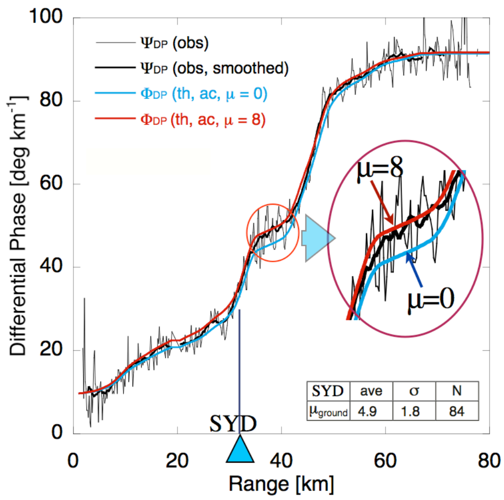

Fig. 4. Radial profiles of observed Ψ_{DP} (thin black line), observed Ψ_{DP} smoothed along 20 gates (thick black line), and theoretical Φ_{DP} with the shape parameters of 0 (light-blue) and 8 (red) for the azimuth of 279° at 0737 JST on 3 December 2010. The blue vertical line indicates the location of a disdrometer at Sekiyado. The mean, standard deviation, and number of samples of the shape parameter derived from the disdrometer data measured on the ground are summarized in the table at the bottom right.

A correction factor of 0.98 dB was applied to the values of measured Z for this profile. This correction factor (C_H) could reflect a bias due to the wet radome of the antenna. Indeed, the correction factor for Z needed to match the two profiles varies with time from 0.00–0.98 dB in the comparisons. This range of bias variation in Z due to a wet radome agrees well with the result of Thompson et al. (2011). In the retrievals of the theoretical Φ_{DP} profiles, we assumed a raindrop temperature of 10 °C and a shape parameter of 5. The temperature was estimated from surface observations at Sekiyado with the dry adiabatic lapse rate, and the value of the shape parameter was estimated by comparing the profiles of smoothed-measured Ψ_{DP} and theoretical Φ_{DP}, as shown below.

In the retrieval of the DSD parameters, we assume that the shape parameter is constant in a range profile, although this assumption may not be satisfied if the radar is sampling mixed convective/stratiform echoes that simultaneously exist in a single profile. Because the shape parameter is one of the parameters that determine the DSD, it influences attenuation, which may affect the profiles of theoretical Φ_{DP}. We found that dependency of the theoretical Φ_{DP} profile on the shape parameter is evident when multiple rainfall peaks existed in a rain path in the radial direction. An example of a Φ_{DP} range profile with attenuation correction procedures is shown in Fig. 4. The gradient of the smoothed-measured Ψ_{DP} profile becomes flat locally with range at around 40 km, suggesting that this range was located between heavy rainfall regions. Note that in that range, the smoothed-measured Ψ_{DP} profile locates between the theoretical Φ_{DP} profiles with shape parameters of 0 and 8, despite the fact that the values of the theoretical Φ_{DP} at the first and last range gates coincide with those of the smoothed-measured Ψ_{DP}. The shape parameter of 5 made all the theoretical Φ_{DP} profiles analyzed in the comparisons fit best with the smoothed-measured Ψ_{DP} profiles associated with the line-shaped convective system. This value may reflect the mean of the shape parameter of this storm. Indeed, the mean value of μ derived from the disdrometer data measured at Sekiyado by the method proposed by Zhang et al. (2003) for the rain associated with the passage of the storm indicates almost the same value, as shown in Fig. 4.

3.3. *Comparison of the Retrieved Microphysical Parameters of Raindrops with Disdrometer Measurements*

To evaluate the reliability of the rain microphysical parameters retrieved with the DSD auto-retrieval technique proposed, we compared these with those derived from the Parsivel disdrometer measurements at Sekiyado, which is located about 31.8 km west–northwest of the MRI site (Fig. 2). Because this type of disdrometer has been reported to have an overestimation tendency, especially in heavy (e.g., R>30 mm h-1) rainfall (e.g., Thurai et al. 2011; Tokay et al. 2013), we reprocessed and applied a quality control to the disdrometer data (for the details, see Appendix A of Adachi et al. (2013)) before the comparisons. The radar-estimated microphysical parameters available for the single point nearest the Sekiyado station were used for the comparisons.

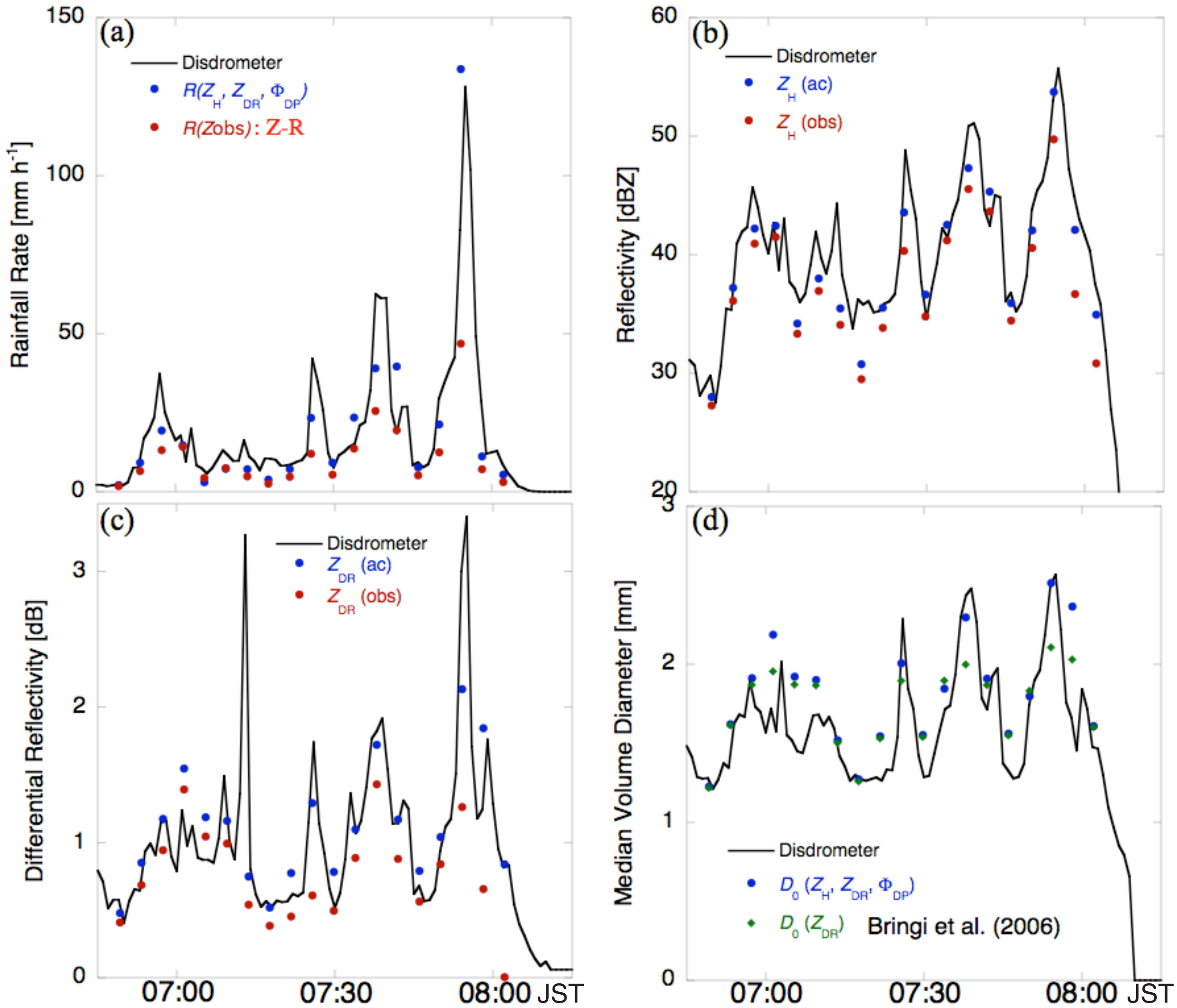

Fig. 5. Time series of (a) rainfall rates, (b) horizontal reflectivities, (c) differential reflectivities, and (d) median volume diameters derived from disdrometer measurements (thick line) and estimated from polarimetric radar data (circles) at the Sekiyado station from 0645 to 0815 JST on 3 December 2010. D_0 (Z_{DR}) in (d) was derived by use of Bringi et al. (2006).

Time series of (a) rainfall rate, (b) reflectivity, (c) differential reflectivity, and (d) median volume diameter derived from the Parsivel and the radar observations at Sekiyado appears in Fig. 5. The thick line shows the 1-min mean data observed with the Parsivel, and the marks in each panel indicate the corresponding data estimated every 4 min from the radar data. The time series of rainfall rate (Fig. 5a) clearly shows that the proposed method $R(Z_H, Z_{DR}, \Phi_{DP})$ outperforms $R(Z\text{obs})$, particularly in heavy rainfall. The reflectivity and differential reflectivity data (Figs. 5b and 5c) show that the observed data have an underestimation tendency, whereas the attenuation-corrected data agree fairly well with the disdrometer observations, despite the large variations in short time. In the comparison of median diameter (Fig. 5d), we plotted an estimation of the median diameter from the relationship proposed by Bringi et al. (2006) as a reference in addition to those derived with the proposed method.

The comparisons show that the parameters derived with the proposed method generally have good agreement with measurements on the ground, suggesting that the DSD estimated with this method is also reliable. A sample comparison of DSD estimated with the proposed method appears in Fig. 6. This comparison was made at the Kumagaya (67.9 km frm the radar) site (Fig. 2) during a passage of typhoon, where attenuation effect was much severer than that of the rain-line event. Black dots represent the DSD data measured on the ground with an Parsivel disdrometer, while thick blue line (dashed red line) represents the DSD estimated with our method (Marchall-Palmer DSD without attenuation correction). Note the DSD derived with the proposed method is represented by a straight line because the value of the shape parameter was estimated to 0. The DSD estimate with our method agrees well with the disdrometers measurements especially for the raindrops with the diameter more than 2 mm. As a result, the estimated rainfall rate is very close to the disdrometers measurements with an error of less than 3% despite large attenuation associated with heavy rainfall. In contrast, the DSD estimated from the measured reflectivity with the radar differs substantially

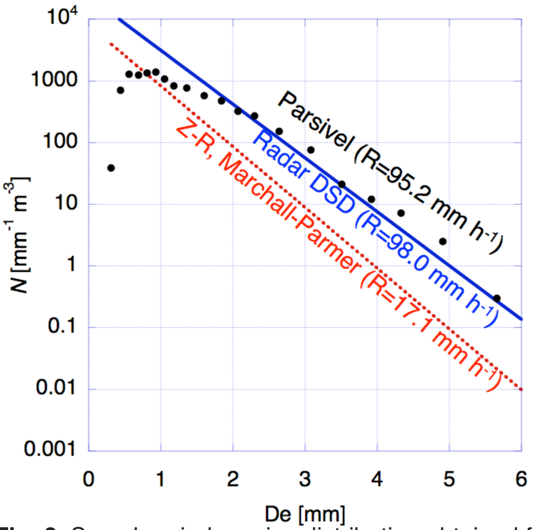

Fig. 6. Sample raindrop size distribution obtained from the disdrometers (black dots) and radar measurements at 1252JST on 21 September 2011 during heavy rainfall associated with a typhoon. The DSD data were estimated both by the proposed method (blue thick line) and by use of the *Z-R* relation and Marchall-Palmer distribution (red dashed-line). Corresponding rainfall rates are indicated along the data in the figure.

from the ground observation. Consequently, the rainfall rate is seriously underestimated (—82%), suggesting unreliability of the estimated rainfall rate based solely on the *Z-R* relation with conventional radar.

4. CONCLUSION

We developed an algorithm for rain attenuation correction of the reflectivity factor and differential reflectivity measured by polarimetric radar at attenuating frequency to retrieve DSD parameters and rainfall rate. It does not require any assumptions of relationship among DSD parameters and/or simplifications of relationship between the axis ratio and diameter of raindrops, which were used in previous studies. Moreover, the proposed algorithm needs no external reference data such as 2DVD measurements for attenuation corrections because it retrieves the co-polar and differential specific attenuation from interrelation among the polarimetric measurements. Additionally, the algorithm retrieves three parameters of the modified gamma distribution, from which rain parameters including rainfall rate can be theoretically estimated.

The performance of this algorithm was evaluated by comparison with optical disdrometers. The evaluation of the algorithm showed fairly good agreement between the retrieved three DSD parameters of raindrops and both reflectivity and differential reflectivity with those obtained by surface measurements. Additionally, the algorithm demonstrated significant improvement in performance for rainfall rate estimation compared with rates estimated using the so-called *Z–R* relationship.

For details of this study, see Adachi et al. (2015).

Acknowledgments

The authors express their appreciation to Prof. Illingworth of University of Reading for his valuable input and guidance on the auto-calibration technique. The authors also thank Prof. Bringi of Colorado State University for providing many helpful comments that improved this work substantially and to Dr. Thurai for many helpful discussions and comments regarding the research presented. The authors are grateful to Dr. Thompson of University of Reading for providing comments on attenuation due to wet radome. The authors thank Dr. Gourley of the NOAA National Severe Storms Laboratory for variable comments on this study. The authors also wish to thank Dr. Ryzhkov of the NOAA National Severe Storms Laboratory for providing information on retrieving shape parameters from disdrometer measurements. This study was partially supported by JSPS KAKENHI Grant Number 15K01273.

References

Adachi, A., T. Kobayashi, and H. Yamauchi, 2015: Estimation of raindrop size distribution and rainfall rate from polarimetric radar measurements at attenuating frequency based on the self-consistency principle. *J. Meteor. Soc. Japan,* **93**, 359-388.

Adachi, A., T. Kobayashi, H. Yamauchi, and S. Onogi, 2013: Detection of potentially hazardous convective clouds with a dual-polarized C-band radar. *Atmos. Meas. Tech.*, **6**, 2741-2760.

Aydin, K., Z. Yang, and T. A. Seliga, 1989: Rain-induced attenuation effects on C-band dual-polarization meteorological radars. *IEEE Trans. Geosci. Remote Sens.*, **27**, 57-66.

Brandes, E. A., G. Zhang, and J. Vivekanandan, 2003: An evaluation of a drop distribution-based polarimetric radar rainfall estimator. *J. Appl. Meteor,* **42**, 652-660.

Bringi, V. N., M. Thurai, K. Nakagawa, G. J. Huang, T. Kobayashi, A. Adachi, H. Hanado, and S. Sekizawa, 2006: Rainfall estimation from C-band polarimetric radar in Okinawa, Japan: Comparison with 2D-video disdrometer and 400 MHz wind profiler. *J. Meteor. Soc. Japan*, **84**, 705-724.

Goddard, J. W. F., J. Tan, and M. Thurai, 1994: Technique for calibration of meteorological radars using differential phase. *Electron. Lett.*, **30**, 166-167.

Gorgucci, E., V. Chandrasekar, V. N. Bringi, and G. Scarchilli, 2002: Estimation of raindrop size distribution parameters from polarimetric radar measurements. *J. Atmos. Sci.*, **59**, 2373-2384.

Gorgucci, E., V. Chandrasekar, and L. Baldini, 2008: Microphysical retrievals from dual-polarization radar measurements at X band. *J. Atmos. Oceanic Technol.*, **25**, 729-741.

Kalogiros, J., M. N. Anagnostou, E. N. Anagnostou, M. Montopoli, E. Picciotti, and F. S. Marzano, 2013: Optimum estimation of rain microphysical parameters from X-band dual-polarization radar observables. *IEEE Trans. Geosci. Remote Sens.*, **51**, 3063-3076.

Löffler-Mang, M., and J. Joss, 2000: An optical disdrometer for measuring size and velocity of hydrometeors. J. Atmos. Oceanic Technol., **17**, 130-139.

Thompson, R., A. Illingworth, and J. Ovens, 2011: Emission: a simple new technique to correct rainfall estimates from attenuation due to both the radome and heavy rainfall. *8th International Symposium on Weather Radar and Hydrology,* Exeter, UK, International Association of Hydrological Sciences, 39-44.

Thurai, M., W. A. Petersen, A. Tokay, C. Schultz, and P. Gatlin, 2011: Drop size distribution comparisons between Parsivel and 2-D video disdrometers. *Adv. Geosci.*, **30**, 3-9.

Tokay, A., W. A. Petersen, P. Gatlin, and M. Wingo, 2013: Comparison of raindrop size distribution measurements by collocated disdrometers. *J. Atmos. Oceanic Technol.,* **30**, 1672-1690.

Zhang, G., J. Vivekanandan, E. A. Brandes, R. Meneghini, and T. Kozu, 2003: The shape-slope relation in observed gamma raindrop size distributions: Statistical error or useful information? *J. Atmos. Oceanic Technol.*, **20**, 1106-1119.